Hindawi
International Transactions on Electrical Energy Systems
Volume 2022, Article ID 4449515, 12 pages
https://doi.org/10.1155/2022/4449515

Research Article

Multi-Time Scale Rolling Optimization Scheduling of "Nealy-Zero Carbon Park" Based on Stepped Carbon Allowance Trading

Tieyan Zhang,[1] **Zongjun Yao**,[1] **Jingwei Hu**,[2] **and Jinfeng Huang**[3]

[1]*School of Electrical Engineering, Shenyang University of Technology, Shenyang 110870, China*
[2]*State Grid Liaoning Power Company Limited Economic Research Institute, Shenyang 110870, China*
[3]*State Grid Shenyang Electric Power Supply Company, Shenyang 110811, China*

Correspondence should be addressed to Zongjun Yao; zjyao@smail.sut.edu.cn

Received 29 June 2022; Revised 3 August 2022; Accepted 5 August 2022; Published 10 September 2022

Academic Editor: Qiuye Sun

Aiming at the self-government capacity and multi-time scale energy regulation requirements of "Nearly-zero Carbon Park" (NZCP) under the background of "dual carbon goals" and energy Internet, a day-ahead-intraday rolling optimization scheduling method for NZCP based on stepped carbon allowance trading is proposed. First, the energy supply and demand characteristics of liquid-storage Carbon Capture Gas-fired Power Plants (CCGPP) and Power-to-Gas (P2G) equipment are studied, and a combined system model of CCGPP and P2G is established that takes into account the low-carbon emission requirements of NZCP, and waste pyrolysis power generation facilities and manure treatment facilities are introduced to form a Waste Utilization system (WU) to provide energy support for the power grid and gas network. Second, the carbon allowance offset and low-carbon benefit gains of NZCP are considered, a compensation coefficient is introduced to guide the low-carbon behavior of carbon emitters, and a ladder carbon allowance trading model is established. Then, the influence of the source-load prediction error on the optimal scheduling at different time scales is considered, and a two-stage unit output plan is established. Then, the influence of the source-load prediction error on the optimal scheduling at different time scales is considered, and a two-stage unit output adjustment plan is established. The calculation example results verify that the proposed day-ahead-intraday rolling optimization scheduling model for NZCP can effectively reduce system carbon emissions while reducing system operating costs, and the efficient integration of economic and environmental benefits is achieved.

1. Introduction

In recent years, with the aggravation of the energy crisis and the greenhouse effect, it has become a global consensus to seek a clean, low-carbon, efficient, and sustainable energy supply method [1–4]. The "14th Five-Year Plan" for the development of bio-economy pointed out to build biomass utilization technology, production, and consumption system [5]. However, with the high proportion of renewable energy access, the multiple uncertainties of source and load and forecast errors have brought severe challenges to the stable operation of NZCP. At the same time, the energy production devices, conversion devices, and energy storage devices in the system have different response times [6–9]. Therefore, the establishment of a flexible operation mode with the ability to adjust at multiple time scales is an important means to deal with the uncertainty caused by the source-load prediction error and ensure the stable operation of the system.

The research on the carbon emission allowance trading mechanism at home and abroad is still in the development stage. Reference [10] studied the fairness of low-carbon economic dispatch in the power system, and proposes an initial allocation method for carbon emission rights based on the idea of a cooperative game. Reference [11] proposed an energy hub model based on carbon allowance trading, and calculates the tiered carbon allowance trading cost according to the carbon emission interval. Reference [12] introduced a

carbon allowance trading mechanism in the comprehensive energy system optimization planning problem, established a reward and punishment ladder-type carbon allowance transaction cost model, and restricted the carbon emission level in the planning area. Most of the above studies focus on using the carbon allowance trading mechanism to control the carbon emission level of the Integrated Energy System. NZCP offsets some carbon emissions through the stepped carbon allowance trading mechanism, so that the difference between carbon sources and carbon allowances is close to zero, and near-zero carbon emissions are achieved while taking into account the benefits brought by the trading mechanism.

At present, some studies have been carried out at home and abroad on the application of biomass utilization technology in integrated energy systems. Reference [13] introduced waste incineration power generation into the urban Integrated Energy System, which improved the adjustment capacity of the power grid and gas grid. Reference [14] proposed the topological structure of the rural multi-energy complex, and established a model of the coordination relationship between the waste stockpile and energy supply. Reference [15] studied the synergistic energy supply characteristics of waste pyrolysis and waste incineration and proposed an urban comprehensive energy system optimization model with waste treatment units. The current research has a relatively simple coupling form for the waste treatment system and has not deeply analyzed the synergistic relationship between the waste treatment system and other energy supply systems.

In order to reduce the power fluctuation caused by the high proportion of renewable energy connected to the new power system and the inconsistent scheduling time scale of each unit in the multi-source energy storage system, a lot of research has been carried out on the day-ahead-intraday multi-time-scale scheduling method in China. Reference [16] established a two-stage predictive optimal scheduling model for the park's comprehensive energy system based on rolling optimization and dynamic adjustment to meet the energy demand of multi-energy users. Reference [17] introduced smart buildings into microgrids to form a virtual energy storage system, and proposed an intraday rolling correction method based on model prediction, which corrects the output deviation of microgrids caused by forecast errors through rolling optimization in different time domains. Reference [18] proposed a multi-time-scale optimal scheduling method for integrated energy systems based on the responsiveness of electric and thermal energy on different time scales to smooth out power fluctuations caused by the uncertainty of renewable energy output.

Through the above analysis, the economic benefits and environmental benefits of tiered carbon allowance trading on NZCP are considered, and a day-ahead-intraday rolling optimization scheduling method is proposed. Day-ahead economic optimal scheduling and intra-day rolling optimal scheduling models were established respectively. Day-ahead economic optimal scheduling determined the optimal output structure, and intra-day rolling optimal scheduling determined the optimal time scale. A power adjustment penalty term is introduced to limit carbon emissions while compensating for carbon emissions, and NZCP's multi-time-scale source-load optimization scheduling is realized. Finally, the simulation verification is carried out via the operation data of the integrated energy system of a park in a certain area in northern China. The calculation example results verify the positive effect of the NZCP multi-time-scale rolling optimization scheduling method proposed in this paper in economic operation and carbon capture.

2. Operational Characteristics and Carbon Cycle Model of NZCP

The NZCP based on tiered carbon allowance trading gives full play to the low-carbon characteristics of zero-carbon resources such as liquid-storage CCGPP and waste utilization systems in the system. At the same time, taking into account the self-regulation level of the load in the system, and controlling the operation status of fixed loads, interruptible loads, and transferable loads through compensation and contracting mechanisms, the energy regulation level of the system can be further improved. However, due to the technical limitations of the carbon capture system, the complete capture of carbon emissions cannot be achieved. Therefore, the carbon allowance offset mechanism is used to achieve near-zero carbon operating characteristics while taking into account the economy. The energy coupling and interaction mode of NZCP is shown in Figure 1.

2.1. CCGPP-P2G System Model. Different from the traditional carbon capture of coal-fired power generating units, the flue gas emitted by gas generating units has higher oxygen content and lower carbon content [19]. Meanwhile, carbon capture systems have high energy consumption characteristics [20]. Therefore, the solution storage CCGPP is adopted, and the carbon capture process is decoupled from the power generation process of the gas power plant by introducing the solution storage carbon capture system, and the energy consumption required for carbon capture is shifted in time and space, thereby improving the consumption capacity of renewable energy while ensuring the energy supply efficiency.

The carbon capture system of solution storage CCGPP consists of a CO_2 capture device and a CO_2 liquefaction device. The flue gas in the absorption tower realizes CO_2 capture through the reverse transmission process with the lean and rich liquid [21]. The electro-carbon characteristics and energy coupling method of carbon capture system are referenced in [22].

It is considered that P2G equipment has good energy space-time transfer characteristics, and P2G equipment is introduced into NZCP and participates in CCGPP joint operation. The CO_2 captured by the carbon capture equipment is used to produce methane, thus providing a good carbon source for CCGPP. The recycling of CO_2 and the improvement of the level of renewable energy consumption are realized, which provides a good margin for the optimal scheduling of the system at multiple time scales [23, 24].

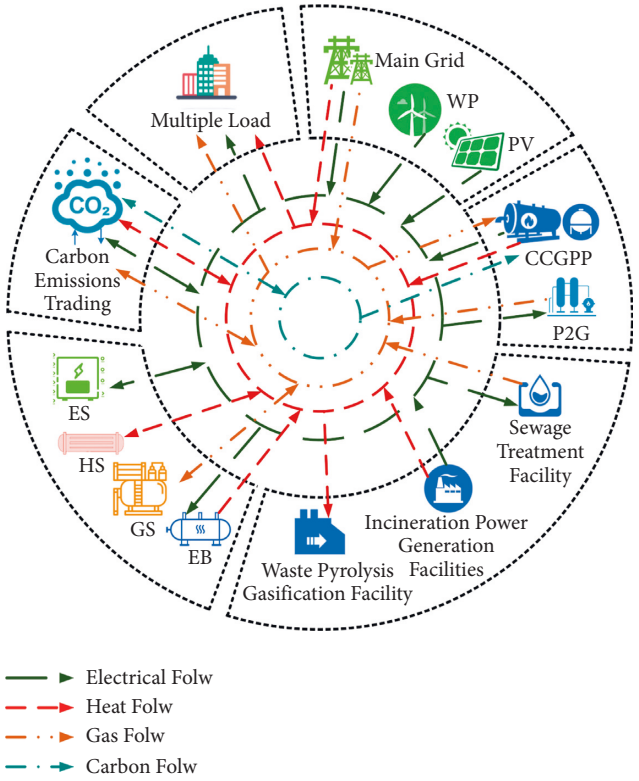

Figure 1: "Nearly-zero carbon park" energy interaction mode.

The energy consumption characteristics of the CCGPP-P2G system can be expressed as:

$$P_{C,CCGPP-P2G,t} = P_{C,CCGPP,t} + P_{C,P2G,t} + P_F, \tag{1}$$

where $P_{C,CCGPP,t}$ is the CCGPP energy consumption at time t, t, $P_{C,P2G,t}$ is the P2G energy consumption at time t, t, and $P_{F,t}$ is the fixed operating energy consumption of the system.

The total amount of CO_2 captured by CCGPP-P2G at time t is $Q^{\Sigma}_{CCGPP-CO_2,t}$, and the total amount of CO_2 consumed in the process of synthesizing methane by P2G is:

$$\begin{aligned} Q^{\Sigma}_{CCGPP-CO_2,t} &= \theta_{CO_2,t}\eta_{CO_2,t}P_{CCGPP,t}, \\ Q^{\Sigma}_{P2G-CO_2,t} &= \chi_{CO_2,t}\eta_{P2G}P_{C,P2G,t}, \end{aligned} \tag{2}$$

where $\theta_{CO_2,t}$ is the carbon emission intensity of processing at time t, t, $\eta_{CO_2,t}$ is the carbon capture rate at time t, t, $P_{CCGPP,t}$ is the total CCGPP output at time t, t, $\chi_{CO_2,t}$ is the amount of CO_2 required to generate unit capacity of natural gas, and η_{P2G} is the gas production efficiency of P2G.

The natural gas production of the CCGPP-P2G system at time t is:

$$P^{\Sigma}_{CCGPP-P2G,G,t} = \frac{3.6\eta_{P2G}P_{C,P2G,t}}{H_g}, \tag{3}$$

where H_g is the calorific value of natural gas.

Due to the high energy consumption characteristics of carbon capture, CCGPP with flue gas diversion is used to control the energy consumption of carbon capture by actively emitting CO_2. The CO_2 discharged into the atmosphere by flue gas diversion is:

$$C_{DE,t} = C_{\Sigma,t} - C_{CCGPP,\Sigma,t}. \tag{4}$$

In the formula, $C_{\Sigma,t}$ is the total amount of CO_2 emitted by all units in the system at time t, t, and $C_{CCGPP,\Sigma,t}$ is the amount of CO_2 captured by CCGPP at time t.

2.2. Waste Utilization System Model. The biomass utilization potential in NZCP is considered, and the WU is proposed to fully dispatch zero-carbon and negative-carbon resources in the NZCP. WU includes waste pyrolysis gasification power generation facilities and manure treatment gas generation facilities.

The waste pyrolysis gasification power generation facility heats and decomposes the sorted organic waste into combustible gas mixed with natural gas by using a high temperature above 800°C [25]. Then, the combustible gas mixed with natural gas is burned to drive the internal combustion engine to generate electricity. The energy supply relationship with waste can be expressed as:

$$P_{WPG,t} = m_{R,t}g_R\eta_P H_F\eta_{F,E}, \tag{5}$$

where $m_{R,t}$ is the input amount of gasifiable waste, g_R is the gasification coefficient, η_P is the calorific value of the gasifiable waste, H_F is the calorific value of the gasified fuel, and $\eta_{F,E}$ is the power generation efficiency of the gas turbine.

The heat energy provided by waste pyrolysis can be expressed as:

$$P_{WPG,H,t} = \frac{P_{WPG,t}\left(1 - \eta_{F,E} - \eta_l\right)}{\eta_{F,E}}\eta_r, \tag{6}$$

where η_l is the heat dissipation loss rate, and η_r is the flue gas recovery rate.

The manure treatment facility makes full use of the sewage and manure resources in the system and uses anaerobic fermentation technology to electrically heat the manure resources and purify them into natural gas, which can be used as a good gas source for CCGPP [26]. For the characteristics of high nitrogen content in manure waste, an appropriate proportion of wet waste is used to adjust the carbon-nitrogen ratio to improve the degree of anaerobic fermentation reaction, thereby increasing gas production [27].

The biogas model for manure treatment facilities can be expressed as:

$$P_{FS,B,t} = m_{FW,t}\eta_{FW,B}\eta_{F,B} + m_{SG,t}\eta_{SG,B}\eta_{S,B}, \tag{7}$$

where $P_{FS,B}$ is the amount of biogas produced by manure treatment, $\eta_{FW,B}$ and $\eta_{SG,B}$ are the treatment efficiency of manure treatment facilities and the treatment efficiency of sewage treatment facilities, respectively, $\eta_{F,B}$ and $\eta_{S,B}$ are the conversion coefficients of manure waste and sewage waste into biogas, and $m_{FW,t}$ and $m_{SG,t}$ are the input amount of manure and sewage, respectively.

After desulfurization and decarbonization, the biogas can be made into natural gas with a purity of more than 90%. Biogas purification of natural gas can be expressed as:

$$P_{\mathrm{FS,G},t} = P_{\mathrm{FS,B},t} a_{\mathrm{F,G}}, \tag{8}$$

where $a_{\mathrm{F,G}}$ is the purification efficiency of biogas.

2.3. Energy Storage Unit Model. The loss characteristics of electrochemical energy storage, hot water tank, and gas storage tank are considered, and the models of Electricity Storage device (ES), Heat Storage device (HS), and Gas Storage device (GS) can be expressed as:

$$\begin{aligned} P_{\mathrm{ES},t} &= \left(1-\ell_{\mathrm{ES}}\right)P_{\mathrm{ES},t-1} + \eta_{\mathrm{ES}}^{\mathrm{ch}} P_{\mathrm{ES},t}^{\mathrm{ch}} - \frac{P_{\mathrm{ES},t}^{\mathrm{dis}}}{\eta_{\mathrm{ES}}^{\mathrm{dis}}}, \\ P_{\mathrm{HS},t} &= \left(1-\ell_{\mathrm{HS}}\right)P_{\mathrm{HS},t-1} + \eta_{\mathrm{HS}}^{\mathrm{ch}} P_{\mathrm{HS},t}^{\mathrm{ch}} - \frac{P_{\mathrm{HS},t}^{\mathrm{dis}}}{\eta_{\mathrm{HS}}^{\mathrm{dis}}}, \\ P_{\mathrm{GS},t} &= \left(1-\ell_{\mathrm{GS}}\right)P_{\mathrm{GS},t-1} + \eta_{\mathrm{GS}}^{\mathrm{ch}} P_{\mathrm{GS},t}^{\mathrm{ch}} - \frac{P_{\mathrm{GS},t}^{\mathrm{dis}}}{\eta_{\mathrm{GS}}^{\mathrm{dis}}}, \end{aligned} \tag{9}$$

where, $P_{\mathrm{ES},t}$, $P_{\mathrm{HS},t}$, and $P_{\mathrm{GS},t}$ are the electricity, heat, and gas energy storage capacity at the end of time t, respectively; ℓ_{ES}, ℓ_{HS}, and ℓ_{GS} are the loss rates of the electricity, heat, and gas energy storage devices themselves; $P_{\mathrm{ES},t-1}$, $P_{\mathrm{HS},t-1}$, and $P_{\mathrm{GS},t-1}$ are the electricity, heat, and gas energy storage at time $t-1$, respectively, the power storage, heat storage, and gas storage; $\eta_{\mathrm{ES}}^{\mathrm{ch}}$, $\eta_{\mathrm{ES}}^{\mathrm{dis}}$ are the charging and discharging efficiency of the power storage device; $P_{\mathrm{ES},t}^{\mathrm{ch}}$, $P_{\mathrm{ES},t}^{\mathrm{dis}}$ are the charging and discharging power of the power storage device at time t; $\eta_{\mathrm{HS}}^{\mathrm{ch}}$, $\eta_{\mathrm{HS}}^{\mathrm{dis}}$ are the charging and discharging efficiency of the heat storage device; $P_{\mathrm{HS},t}^{\mathrm{ch}}$, $P_{\mathrm{HS},t}^{\mathrm{dis}}$ are the charging and discharging power of the heat storage device at time t; $\eta_{\mathrm{GS}}^{\mathrm{ch}}$, $\eta_{\mathrm{GS}}^{\mathrm{dis}}$ are the charging and degassing efficiency of the gas storage device; and $P_{\mathrm{GS},t}^{\mathrm{ch}}$, $P_{\mathrm{GS},t}^{\mathrm{dis}}$ are the charging and degassing power of the gas storage device at time a.

2.4. Multi-Energy Coupling Energy Flow Model. NZCP includes a variety of energy production and transportation forms, and the multi-source coordination method is described by the coupling matrix as:

$$\begin{bmatrix} P_{\mathrm{EL},t} \\ P_{\mathrm{HL},t} \\ P_{\mathrm{GL},t} \end{bmatrix} = \begin{bmatrix} P_{\mathrm{EW},t} \\ P_{\mathrm{HW},t} \\ P_{\mathrm{GW},t} \end{bmatrix} + \begin{bmatrix} P_{\mathrm{ES},t} \\ P_{\mathrm{HS},t} \\ P_{\mathrm{GS},t} \end{bmatrix} + \begin{bmatrix} 1-\alpha_1-\alpha_2 & g_{\mathrm{R}}\eta_{\mathrm{P}}H_{\mathrm{F}}\eta_{\mathrm{F,E}} & 0 & 0 & \eta_{\mathrm{CCGPP}} \\ \alpha_1\eta_{\mathrm{EB}} & g_{\mathrm{R}}\eta_{\mathrm{P}}H_{\mathrm{F}}\eta_{\mathrm{F,E}}\dfrac{\left(1-\eta_{\mathrm{F,E}}-\eta_1\right)\eta_{\mathrm{r}}}{\eta_{\mathrm{F,E}}} & 0 & 0 & \eta_{\mathrm{CCGPP,H}} \\ \alpha_2\eta_{\mathrm{P2G}} & 0 & \eta_{\mathrm{FW,B}}\eta_{\mathrm{F,B}}a_{\mathrm{F,G}} & \eta_{\mathrm{SG,B}}\eta_{\mathrm{S,B}}a_{\mathrm{F,G}} & 0 \end{bmatrix} \begin{bmatrix} P_{\mathrm{WP},t}+P_{\mathrm{PV},t} \\ m_{\mathrm{R},t} \\ m_{\mathrm{FW},t} \\ m_{\mathrm{SG},t} \\ P_{\mathrm{CCGPP},t} \end{bmatrix}, \tag{10}$$

where $P_{\mathrm{EL},t}$, $P_{\mathrm{HL},t}$, and $P_{\mathrm{GL},t}$ are the loads of electricity, heat and gas, respectively; $P_{\mathrm{EW},t}$, $P_{\mathrm{HW},t}$, and $P_{\mathrm{GW},t}$ are the electricity, heat, and gas power purchased from the main network, respectively; $P_{\mathrm{WP},t}$ and $P_{\mathrm{PV},t}$ are the on-grid power of wind power and the on-grid power of photovoltaics, respectively; and η_{CCGPP}, $\eta_{\mathrm{CCGPP,H}}$, η_{EB}, and η_{P2G} are the CCGPP power supply efficiency, CCGPP thermoelectric ratio, EB heating efficiency, and P2G gas supply efficiency, respectively.

3. Ladder Carbon Allowance Trading Model

Carbon emission allowance trading is a legal carbon emission allowance allocated to each energy producer or integrated energy body under the premise of environmental and market factors. If the actual carbon emission of the energy producer is higher than the carbon emission allowance in the production process, it needs to purchase the corresponding amount of carbon emission allowance from the carbon emission trading market. Conversely, if the actual carbon emission of the energy producer is higher than the carbon emission allowance in the production process, the corresponding allowance can be sold in the carbon emission rights trading market to obtain low-carbon benefits. The NZCP can offset carbon emissions with appropriate carbon emission rights allowances, so that the carbon emission level in the system is within a constraint range to achieve near-zero carbon emissions.

The management department allocates the initial carbon emission right pre-allowance based on the carbon emissions of each energy-producing entity or integrated energy body in the previous year, and then determines the actual initial

allowance based on the actual energy supply after accounting. In this paper, carbon emissions and carbon emission allowances are liquidated on an hourly time scale.

The carbon emission rights participating in the carbon allowance trading market is:

$$\begin{aligned} P_{\mathrm{T},t} &= P_{\mathrm{DE},t} - P_{\mathrm{EMI},t}, \\ P_{\mathrm{DE},t} &= \varpi_{\mathrm{CCGPP}} P_{\mathrm{CCGPP},t} + \varpi_{\mathrm{WPG}} P_{\mathrm{WPG},t} \\ &\quad - \theta_{\mathrm{CO_2}} P^{\Sigma}_{\mathrm{CCGPP-P2G,G},t}, \\ P_{\mathrm{EMI},t} &= \partial_1 P_{\mathrm{CCGPP},t} + \partial_2 P_{\mathrm{WPG},t} + \partial_3 P_{\mathrm{WPG,H},t}, \end{aligned} \tag{11}$$

where $P_{\mathrm{DE},t}$ and $P_{\mathrm{EMI},t}$ are the system CO_2 net carbon emissions and free carbon emission rights, respectively; ϖ_{CCGPP}, ϖ_{CCGPP} and ϖ_{WPG} are the carbon emission intensity corresponding to the unit natural gas consumed by CCGPP, and the carbon emission intensity corresponding to the incineration power generation per unit of waste pyrolysis gasification; $\theta_{\mathrm{CO_2}}$ is the CO_2 density; ∂_1, ∂_2, and ∂_3 are the carbon emission rights allocation quota corresponding to the unit power supply of CCGPP, power supply after waste pyrolysis and gasification, and heating power, respectively.

Different from the traditional unified reward and punishment carbon allowance trading mechanism, the tiered price trading mechanism is introduced in this paper, which is analogous to the time-of-use energy price and establishes a transaction cost calculation method based on the carbon emission range. When the carbon emissions of energy producers exceed the constraint range, the price of carbon allowances rises in stages. At the same time, a compensation coefficient is introduced to motivate the low-carbon behavior compensation of energy-producing subjects [10].

The tiered carbon allowance transaction costs are:

$$C_{\mathrm{CO_2}} = \begin{cases} p_{\mathrm{B}} P_{\mathrm{T},t}, & L \le P_{\mathrm{T},t}, \\ p_{\mathrm{B}} L + p_{\mathrm{B}}\left(P_{\mathrm{T},t} - L\right)(1+\phi), & L < P_{\mathrm{T},t} \le 2L, \\ p_{\mathrm{B}}(2+\phi)L + p_{\mathrm{B}}\left(P_{\mathrm{T},t} - L\right)(1+2\phi), & 2L < P_{\mathrm{T},t} \le 3L, \\ p_{\mathrm{B}}(3+3\phi)L + p_{\mathrm{B}}\left(P_{\mathrm{T},t} - L\right)(1+3\phi), & 3L < P_{\mathrm{T},t} \le 4L, \\ p_{\mathrm{B}}(4+6\phi)L + p_{\mathrm{B}}\left(P_{\mathrm{T},t} - L\right)(1+4\phi), & P_{\mathrm{T},t} > 4L, \end{cases} \tag{12}$$

where p_{B} is the base price of carbon allowance trading; L is the length of the carbon emission range; and ϕ is the compensation factor. When $P_{\mathrm{T},t} > 0$, it means that the actual carbon emission of the system is lower than the free carbon emission, and the remaining part of the allowance can participate in the trading market to obtain benefits.

4. NZCP Multi-Time Scale Rolling Optimization Scheduling Strategy

The traditional day-ahead scheduling method is difficult to effectively deal with the source-load forecast error and multiple uncertainties of NZCP. Tiered carbon allowance trading and various equipment operation constraints are considered, and a multi-time scale rolling optimization model is established. The hour-level time resolution is selected, and the optimization goal is to minimize the daily operating cost of the system, and formulate the optimal output and adjustment plan of the unit throughout the day.

Intraday scheduling is to formulate the unit output plan according to the previous scheduling stage, select 15 min as the time scale for rolling optimization, based on the results of renewable energy generation and short-term multi-load forecasting. Through continuous rolling optimization to ensure the accuracy and effectiveness of the dispatch plan, the optimal state adjustment of the source, load, and output is realized.

The day-ahead-intraday rolling optimization strategy framework is shown in Figure 2. Among them, t is the scheduling period, Δt is the scheduling time interval, H is the rolling time domain, and n is the total number of time periods in the rolling time domain.

4.1. Day-Ahead Optimization. The objective function of the day-ahead scheduling phase is:

$$\begin{aligned} &\min\left(C_{\mathrm{buy}} + C_{\mathrm{WP,PV}} + C_{\mathrm{P2G}} + C_{\mathrm{WU}} + C_{\mathrm{CCGPP}} \right. \\ &\quad \left. + C_{\mathrm{EB}} + C_{\mathrm{CSE}} + C_{\mathrm{CO_2}} + C_{\mathrm{L,DR}}\right), \\ C_{\mathrm{buy}} &= \sum_{t=1}^{T} \partial_{\mathrm{E},t} P_{\mathrm{EW}} + \sum_{t=1}^{T} \partial_{\mathrm{H},t} P_{\mathrm{HW}} + \sum_{t=1}^{T} \partial_{\mathrm{G},t} P_{\mathrm{GW}}, \\ C_{\mathrm{WP,PV}} &= \sum_{t=1}^{T} \gamma_{\mathrm{WP},t} P_{\mathrm{WP}} + \sum_{t=1}^{T} \gamma_{\mathrm{PV},t} P_{\mathrm{PV}}, \\ C_{\mathrm{P2G}} &= \sum_{t=1}^{T} \gamma_{\mathrm{P2G},t} P_{\mathrm{C,P2G},t}, \\ C_{\mathrm{WU}} &= \sum_{t=1}^{T} \left[a_1 + b_1\left(m_{\mathrm{R},t} + m_{\mathrm{FW}} + m_{\mathrm{SG}}\right) \right. \\ &\quad \left. + c_1\left(m_{\mathrm{R},t} + m_{\mathrm{FW}} + m_{\mathrm{SG}}\right)^2\right], \\ C_{\mathrm{CCGPP}} &= \sum_{t=1}^{T} \gamma_{\mathrm{CCGPP},t} P_{\mathrm{CCGPP},t}, \\ C_{\mathrm{EB}} &= \sum_{t=1}^{T} \gamma_{\mathrm{EB},t} P_{\mathrm{EB},t}, \\ C_{\mathrm{CSE}} &= \sum_{t=1}^{T} \gamma_{\mathrm{CSE},t} Q_{\mathrm{CSE,CO_2},t}, \\ C_{\mathrm{L,DR}} &= \sum_{t=1}^{T} \sum_{k}^{K} b_{k,\mathrm{int},t} P^{\mathrm{int}}_{k,\mathrm{DR},t} + \sum_{t=1}^{T} b_{\mathrm{shi},t} P^{\mathrm{shi}}_{\mathrm{DR},t}, \end{aligned} \tag{13}$$

where C_{buy}, $C_{\mathrm{WP,PV}}$, C_{P2G}, C_{WU}, C_{CCGPP}, C_{EB}, C_{CSE}, $C_{\mathrm{CO_2}}$, and $C_{\mathrm{L,DR}}$ are the energy purchase cost, operation and maintenance cost of renewable energy power generation equipment, P2G unit operation cost, waste utilization system operation cost, CCGPP operation cost, EB unit operation cost, carbon sequestration cost, tiered carbon allowance transaction cost, and demand-side response load compensation cost, respectively; $\partial_{\mathrm{E},t}$, $\partial_{\mathrm{H},t}$, and $\partial_{\mathrm{G},t}$ are the electricity price, heat price, and natural gas price at the moment; $\gamma_{\mathrm{WP},t}$,

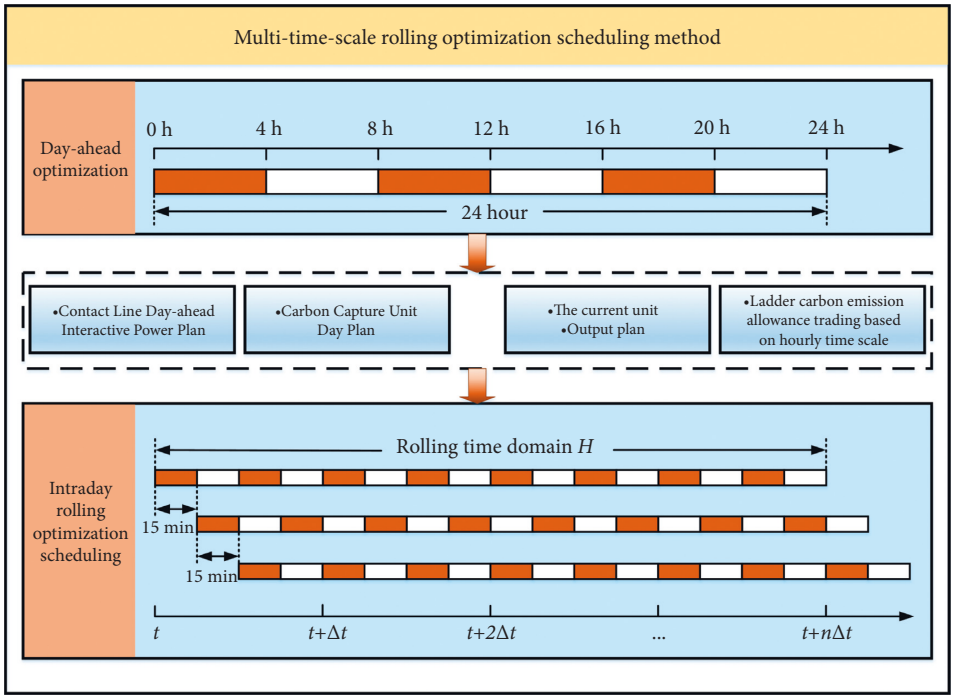

Figure 2: Multi-time scale rolling optimization scheduling framework.

$\gamma_{PV,t}$are the unit operation and maintenance costs of wind power and photovoltaics at the moment, respectively; $\gamma_{P2G,t}$, $\gamma_{EB,t}$ are the operating cost coefficients of P2G units and EB units, respectively; a_1, b_1, c_1 are the operating cost coefficients of the waste utilization system; $\gamma_{CCGPP,t}$ is the CCGPP operating cost coefficient; $\gamma_{CSE,t}$ is the unit cost of carbon sequestration; $Q_{CSE,CO_2,t}$ is the amount of CO_2 sequestered by the carbon sequestration device; k is the number of interruption levels; $P^{int}_{k,DR,t}$ and $b_{k,int,t}$ are respectively the k-th level of interruption load and the interruption compensation price; $P^{shi}_{DR,t}$ and $b_{shi,t}$ are respectively the transferable load and the transferable load compensation price.

4.2. Constraints

(1) Power balance constraints:

$$\begin{aligned}
&P_{EW,t} + P_{WP,t} + P_{PV,t} + P_{WPG,t} + P_{CCGPP,E,t} - P_{C,CCGPP-P2G,t} - \\
&P_{P2G,t} + P^{dis}_{ES,t} - P_{FS,E,t} - P_{EB,t} = P^{ch}_{ES,t} + P_{EL,t}, \\
&P_{HW,t} + P_{WPG,H,t} + P_{CCGPP,H,t} + P^{H}_{EB,t} + P^{dis}_{HS,t} = P^{ch}_{HS,t} + P_{HL,t}, \\
&P_{GW,t} + P_{FS,G,t} + P_{P2G,H,t} + P^{\Sigma}_{CCGPP-P2G,G,t} - P_{CCGPP,t} + P^{dis}_{GS,t} \\
&= P^{ch}_{GS,t} + P_{GL,t},
\end{aligned} \tag{14}$$

where $P_{EW,t}$, $P_{HW,t}$, and $P_{GW,t}$ are the electricity, heat, and gas power purchased from the main grid, respectively; $P_{WP,t}$, $P_{PV,t}$ are the wind power on-grid power and photovoltaic on-grid power, respectively; $P_{EL,t}$, $P_{HL,t}$, and $P_{GL,t}$ are the electricity, heat, and gas loads, respectively.

(2) CCGPP operating constraints:

$$0 \le P_{CCGPP,t} \le P_{CCGPP,max}, \tag{15}$$

where $P_{CCGPP,max}$ is the upper limit of CCGPP output.

(3) Operational constraints of Waste Utilization system:

The operational constraints of waste pyrolysis gasification power generation facilities can be expressed as:

$$P^{min}_{WPG,t} \le P_{WPG,t} \le P^{max}_{WPG,t}, \tag{16}$$

where $P^{max}_{WPG,t}$ and $P^{min}_{WPG,t}$ are the upper limit and lower limit of power supply power for waste pyrolysis and gasification, respectively.

The operation constraints of manure treatment equipment can be expressed as:

$$\begin{aligned}
\Delta P_{FS,G,min} \le P_{FS,G,t} - P_{FS,G,t-1} \le \Delta P_{FS,G,max}, \\
P^{min}_{FS,G,t} \le P_{FS,G,t} \le P^{max}_{FS,G,t},
\end{aligned} \tag{17}$$

where $P^{max}_{FS,G,t}$ and $P^{min}_{FS,G,t}$ are the upper and lower limits of the manure treatment power, respectively; $\Delta P_{FS,G,max}$ and $\Delta P_{FS,G,min}$ are the upper and lower limits of the climbing rate of the manure treatment equipment, respectively.

(4) P2G operation constraints:

$$\begin{aligned}
0 \le P_{C,P2G,t} \le P_{P2G,max}, \\
\Delta P_{P2G,min} \le P_{P2G,t+1} - P_{P2G,t} \le \Delta P_{P2G,max},
\end{aligned} \tag{18}$$

where $P_{\mathrm{P2G,max}}$ is the upper limit of the P2G output; $\Delta P_{\mathrm{P2G,max}}$ and $\Delta P_{\mathrm{P2G,min}}$ are the upper and lower limits of the P2G ramp rate, respectively.

(5) Electric Boiler operation constraints:

$$\begin{aligned} 0 \le P_{\mathrm{EB},t} \le P_{\mathrm{EB,max}}, \\ \Delta P_{\mathrm{EB,min}} \le P_{\mathrm{EB},t+1} - P_{\mathrm{EB},t} \le \Delta P_{\mathrm{EB,max}}, \end{aligned} \tag{19}$$

where $P_{\mathrm{EB,max}}$ is the upper limit of EB output; $\Delta P_{\mathrm{EB,max}}$ and $\Delta P_{\mathrm{EB,min}}$ are the upper limit and lower limit of the EB ramp rate constraint, respectively.

(6) Energy storage devices operation constraints:

$$\begin{aligned} 0 \le P_{\mathrm{ES},t}^{\mathrm{ch}} \le P_{\mathrm{ES},t}^{\mathrm{ch,max}} o_{\mathrm{ES},t}^{\mathrm{ch}}, \\ 0 \le P_{\mathrm{ES},t}^{\mathrm{dis}} \le P_{\mathrm{ES},t}^{\mathrm{dis,max}} o_{\mathrm{ES},t}^{\mathrm{dis}}, \\ 0 \le o_{\mathrm{ES},t}^{\mathrm{ch}} + o_{\mathrm{ES},t}^{\mathrm{dis}} \le 1, \\ P_{\mathrm{ES},t}^{\mathrm{min}} \le P_{\mathrm{ES},t} \le P_{\mathrm{ES},t}^{\mathrm{max}}, \end{aligned} \tag{20}$$

where $P_{\mathrm{ES},t}^{\mathrm{ch,max}}$ and $P_{\mathrm{ES},t}^{\mathrm{dis,max}}$ are the maximum value of the charging and discharging power of the power storage device, respectively; $o_{\mathrm{ES},t}^{\mathrm{ch}}$ and $o_{\mathrm{ES},t}^{\mathrm{dis}}$ are the charging and discharging states of the power storage device, respectively. In case of $o_{\mathrm{ES},t}^{\mathrm{ch}} = 0$, $o_{\mathrm{ES},t}^{di\ s} = 1$, the system is in a state of discharge, and in case of $o_{\mathrm{ES},t}^{\mathrm{ch}} = 1 o_{\mathrm{ES},t}^{\mathrm{dis}} = 0$, the system is in a state of charge; $P_{\mathrm{ES},t}^{\mathrm{max}}$ and $P_{\mathrm{ES},t}^{\mathrm{min}}$ are the maximum and minimum storage capacity of the power storage device, respectively. The heat storage device and the gas storage device are the same.

(7) Tie line power constraints:

$$\begin{aligned} P_{\mathrm{EW},t,\mathrm{min}} \le P_{\mathrm{EW},t} \le P_{\mathrm{EW},t,\mathrm{max}}, \\ P_{\mathrm{HW},t,\mathrm{min}} \le P_{\mathrm{HW},t} \le P_{\mathrm{HW},t,\mathrm{max}}, \\ P_{\mathrm{GW},t,\mathrm{min}} \le P_{\mathrm{GW},t} \le P_{\mathrm{GW},t,\mathrm{max}}. \end{aligned} \tag{21}$$

In the formula, $P_{\mathrm{EW},t,\mathrm{max}}$ and $P_{\mathrm{EW},t,\mathrm{min}}$ are the maximum and minimum power of the tie line between the system and the power grid, respectively; $P_{\mathrm{HW},t,\mathrm{max}}$ and $P_{\mathrm{HW},t,\mathrm{min}}$ are the maximum and minimum power of the tie line between the system and the heat grid, respectively; $P_{\mathrm{GW},t,\mathrm{max}}$, $P_{\mathrm{GW},t,\mathrm{min}}$ are the maximum and minimum power of the tie line between the system and the gas network, respectively.

4.3. Intraday Rolling Optimization

$$\begin{aligned} &\min\left(C_{\mathrm{buy,roll}} + C_{\mathrm{WU,roll}} + C_{\mathrm{CCGPP,roll}} C_{\mathrm{ES,roll}} + C_{\mathrm{HS,roll}} + C_{\mathrm{GS,roll}}\right), \\ C_{\mathrm{buy,roll}} &= \sum_{t=1}^{T} \partial_{\mathrm{E},t}\left(P_{\mathrm{EW},\Theta,t} + \Delta P_{\mathrm{EW},t}\right) + \partial_{\mathrm{E,pu},t}\left(\Delta P_{\mathrm{EW},t}\right)^2 \\ &\quad + \sum_{t=1}^{T} \partial_{\mathrm{H},t}\left(P_{\mathrm{HW},\Theta,t} + \Delta P_{\mathrm{HW},t}\right) + \partial_{\mathrm{H,pu},t}\left(\Delta P_{\mathrm{HW},t}\right)^2 + \sum_{t=1}^{T} \partial_{\mathrm{G},t}\left(P_{\mathrm{GW},\Theta,t} + \Delta P_{\mathrm{GW},t}\right) + \partial_{\mathrm{G,pu},t}\left(\Delta P_{\mathrm{GW},t}\right)^2, \\ C_{\mathrm{WU,roll}} &= \sum_{t=1}^{T} \left[\begin{array}{l} a_1 + b_1\left(m_{\mathrm{R},\Theta,t} + m_{\mathrm{FW},\Theta} + m_{\mathrm{SG},\Theta} + \Delta m_{\mathrm{R},t} + \Delta m_{\mathrm{FW}} + \Delta m_{\mathrm{SG}}\right) \\ \quad + c_1\left(m_{\mathrm{R},\Theta,t} + m_{\mathrm{FW},\Theta} + m_{\mathrm{SG},\Theta} + \Delta m_{\mathrm{R},t} + \Delta m_{\mathrm{FW}} + \Delta m_{\mathrm{SG}}\right)^2 \end{array} \right], \\ C_{\mathrm{CCGPP,roll}} &= \sum_{t=1}^{T} \gamma_{\mathrm{CCGPP},t}\left(P_{\mathrm{CCGPP},t} + \Delta P_{\mathrm{CCGPP},t}\right), \\ C_{\mathrm{ES,roll}} &= \sum_{t=1}^{T} \partial_{\mathrm{E},t}\left(\Delta P_{\mathrm{ES},t}^{\mathrm{ch}}\right)^2 + \partial_{\mathrm{E},t}\left(\Delta P_{\mathrm{ES},t}^{\mathrm{dis}}\right)^2, \\ C_{\mathrm{HS,roll}} &= \sum_{t=1}^{T} \partial_{\mathrm{H},t}\left(\Delta P_{\mathrm{HS},t}^{\mathrm{ch}}\right)^2 + \partial_{\mathrm{H},t}\left(\Delta P_{\mathrm{HS},t}^{\mathrm{dis}}\right)^2, \\ C_{\mathrm{GS,roll}} &= \sum_{t=1}^{T} \partial_{\mathrm{G},t}\left(\Delta P_{\mathrm{GS},t}^{\mathrm{ch}}\right)^2 + \partial_{\mathrm{G},t}\left(\Delta P_{\mathrm{GS},t}^{\mathrm{dis}}\right)^2, \end{aligned} \tag{22}$$

where $C_{\mathrm{buy,roll}}$, $C_{\mathrm{WU,roll}}$, $C_{\mathrm{CCGPP,roll}}$, $C_{\mathrm{ES,roll}}$, $C_{\mathrm{HS,roll}}$, and $C_{\mathrm{GS,roll}}$ are the cost of purchasing energy from the main network during rolling optimization, the operating cost of the waste utilization system, the operating cost of CCGPP, penalty cost of charging and discharging power change of electric storage device, penalty cost of charging and discharging power fluctuation of heat storage device, and penalty cost of charging and discharging power fluctuation of gas storage device, respectively; $P_{\mathrm{EW},\Theta,t}$, $P_{\mathrm{HW},\Theta,t}$, and $P_{\mathrm{GW},\Theta,t}$ are the power, heat, and gas purchased from the main network a few days ago, respectively; $\Delta P_{\mathrm{EW},t}$, $\Delta P_{\mathrm{HW},t}$, and $\Delta P_{\mathrm{GW},t}$ are the power, heat, and gas adjustment power

purchased within the day, respectively; $m_{R,\Theta,t}$, $m_{FW,\Theta}$, and $m_{SG,\Theta}$ are the input amount of organic waste, feces, and sewage after the previous classification, respectively; $\Delta m_{R,t}$, Δm_{FW}, and Δm_{SG} are the adjusted amount of organic waste, feces, and sewage after the classification within the day, respectively; $\Delta P_{CCGPP,t}$ is the daily adjustment power of CCGPP, respectively; $\Delta P^{ch}_{ES,t}$ and $\Delta P^{dis}_{ES,t}$ are the adjustment amounts of the charging and discharging power of the power storage device, respectively; $\Delta P^{ch}_{HS,t}$ and $\Delta P^{dis}_{HS,t}$ are the adjustment amounts of the charging and discharging power of the heat storage device, respectively; $\Delta P^{ch}_{GS,t}$, $\Delta P^{dis}_{GS,t}$ are the adjustment amounts of the gas storage device charging and discharging power, respectively.

5. Case Analysis

The NZCP multi-time-scale optimization model based on stepped carbon allowance trading established in this study is a typical mixed integer linear programming problem, the Yalmip + Cplex solver is used to solve the problem based on the MATLAB platform.

In this paper, an example simulation is carried out by taking a Park-level Integrated Energy System in northern my country as an example. Renewable energy power generation and multiple load forecast curves are shown in Figure 3. The parameters of each device are shown in Table 1.

In order to verify the economy and low-carbon characteristics of the NZCP multi-time-scale rolling optimization scheduling method based on the ladder carbon allowance trading mechanism proposed in this study, the following three scenarios are used to compare and analyze NZCP. In Scenario 1, the carbon allowance trading mechanism is not considered, and the conventional day-ahead scheduling method is adopted. In Scenario 2, a unified carbon allowance trading mechanism is introduced, and the conventional day-ahead scheduling method is adopted. In Scenario 3, the stepped carbon allowance trading mechanism proposed in this paper is introduced, and the multi-time-scale rolling optimization scheduling method proposed in this paper is adopted. The basic parameters of carbon allowance trading are set: the base price is 250 yuan/t, the compensation coefficient is 0.25, the carbon emission interval length $L = 50$ t, and the carbon allowance price growth rate is 25%. The scheduling results and carbon emissions under the three scenarios are shown in Table 2.

It can be seen that the introduction of unified carbon allowance trading in Scenario 2 effectively restrains the CO_2 emission level of production enterprises, and the CO_2 emission is reduced by 711.56 t compared with Scenario 1. However, due to the lack of effective output adjustment methods and optimal scheduling mechanisms for the high energy consumption characteristics of carbon capture equipment in Scenario 2, the cost of energy purchase and carbon sequestration will increase, and the unified carbon allowance trading lacks effective reward, punishment and incentive policies, the cost of Scenario 2 increases by 6.39% compared to Scenario 1.

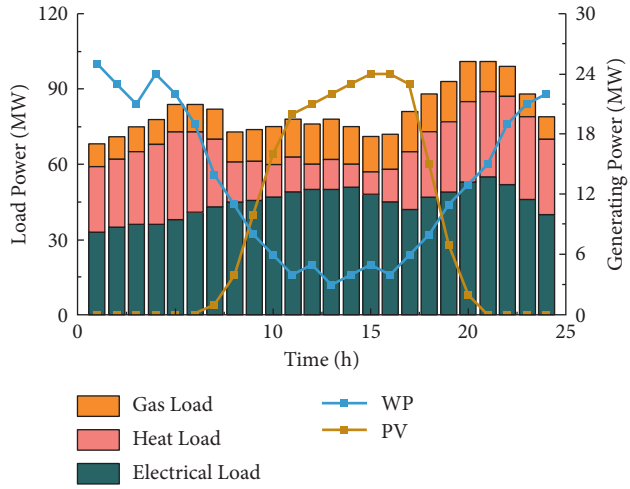

Figure 3: Renewable energy generation and load forecast curve.

The tiered carbon allowance trading further constrains the CO_2 emission level of production enterprises. Compared with Scenario 2, the CO_2 emission of Scenario 3 is reduced by 4.76 t, achieving near-zero carbon emissions in the NZCP system. At the same time, the step-by-step allowance price mechanism adopted in Scenario 3 encourages production enterprises to obtain low-carbon behavior benefits, which reduces operating costs by 21.51% and 26.23%, respectively, compared with Scenario 1 and Scenario 2. Benefiting from the tiered carbon allowance trading mechanism, the revenue is greater than the expenditure brought by carbon capture and storage, which verifies that the scheduling method proposed in this study takes into account the reduction of carbon emissions and the reduction of operating costs.

5.1. Day-Ahead Scheduling Result Analysis. Figures 4–6 show the optimal scheduling results of the proposed operation mode for the power grid, heat grid, and gas grid based on Scenario 3. The load peak period is 18 h–22 h and 8 h–9 h. At this time, CCGPP is mainly responsible for providing energy consumption for the load. At the same time, the waste pyrolysis and gasification power generation facilities provide active support for the power grid, the carbon emissions at this time are transferred into the liquid storage device through the flue gas bypass. During the period of 10 h–16 h and 22 h–4 h, the electrical load is in low period, and renewable energy is mainly used to generate electricity to meet the energy consumption of carbon capture in the liquid storage equipment. It can be seen that CCGPP and waste utilization system smooth the peak-to-valley curve of electrical load, and liquid storage CCGPP provides a good way for renewable energy consumption.

During the period of 11 h–14 h and 17 h–20 h, it is in the peak period of gas consumption. At this time, the manure gas production facilities in the waste utilization system increase the output, which not only increases the peak shaving capacity of the gas network, but also provides a stable gas source for CCGPP. It can be seen that the waste utilization system can provide peak shaving capability for the gas

Table 1: The operating parameters of each equipment.

Equipment	Parameter	Numerical value
Waste pyrolysis gasification power generation facility	Amount of garbage handled	40
	Rated power	30
Manure treatment facility	The amount of manure treated	40
P2G	Electric to gas efficiency	0.7
	Output climbing upper and lower limit	10/0
EB	Electricity to heat efficiency	0.6
	Output climbing upper and lower limit	10/0
Electricity storage device	Maximum charge and discharge power	25/25
	Charge/discharge factor	0.9/0.9
Heat storage device	Maximum charge and discharge power	10/10
	Charge/discharge factor	0.9/0.9
Gas storage device	Maximum charge and discharge power	4/4
	Charge/discharge factor	0.9/0.9

Table 2: Optimization results in each scenario and carbon emissions after allowance offset.

Type	Scenario 1	Scenario 2	Scenario 3
Energy purchase cost	6.77	7.32	6.63
Operation and maintenance costs of renewable energy power generation equipment	1.51	1.78	1.35
Waste utilization system operating costs	3.23	3.23	3.23
CCGPP operating cost	4.72	5.13	5.41
P2G unit operating cost	0.72	0.93	0.95
Carbon sequestration cost	0.11	0.25	0.33
Carbon allowance transaction cost	0	-0.51	-4.51
CO_2 emissions after allowance offset	752.14	40.58	8.99
Total operating cost	17.06	18.15	13.39

Unit: 10^4 ¥.

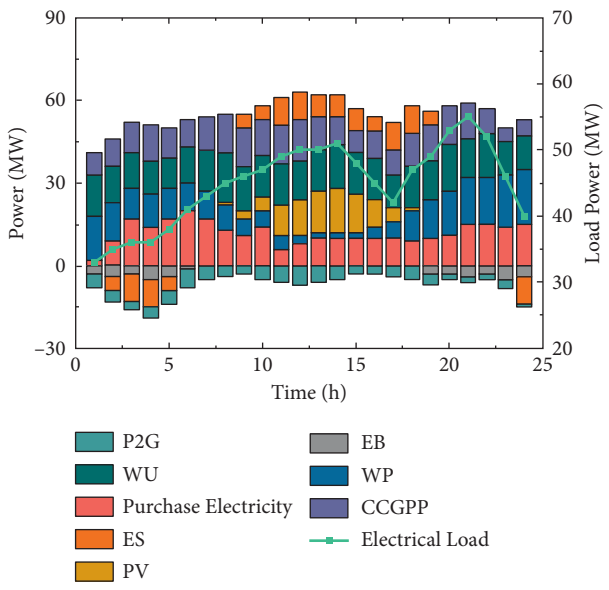

Figure 4: Electricity dispatch results.

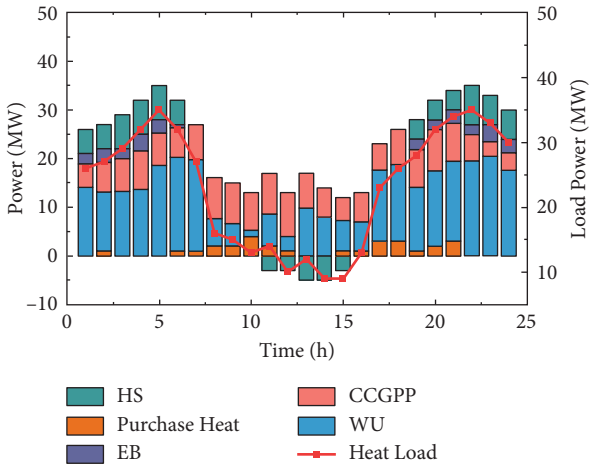

Figure 5: Heat dispatch results.

network, and the operating cost is low. It provides a good adjustment capability for the gas network and effectively reduces the operating cost of the system.

5.2. Analysis of Intraday Scheduling Results. The optimal rolling optimization duration within the day is determined based on the operation method proposed in Scenario 3. The system operating costs under different rolling optimization durations are shown in Figure 7.

It can be seen that when the rolling optimization time is increased from 1 h to 3 h, the operating cost is increased from 16.97×10^4 ¥ to 27.74×10^4 ¥; when the rolling optimization time is increased from 3 h to 4 h, the operating cost

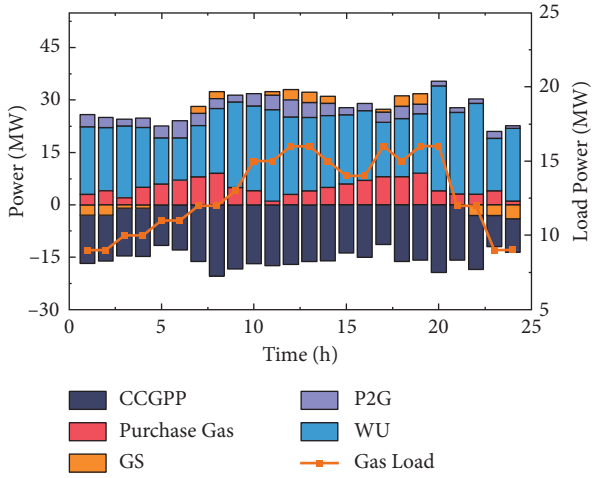

Figure 6: Gas dispatch results.

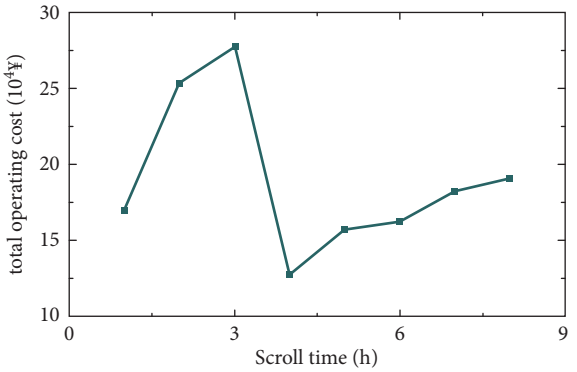

Figure 7: The total operating cost curve of the system under different rolling optimization durations.

is reduced from 27.74×10^4¥ to 12.74×10^4¥; when the rolling optimization time is increased from 5 h to 8 h, the operating cost increases from 15.69×10^4¥ to 19.07×10^4¥. According to the above optimization operation results, when the rolling optimization time is 4 h, the system operating cost is reduced by 4.85% compared with the previous total operating cost, and the goal of minimum operating cost is achieved. It can be seen that the optimal rolling optimization time H is 4 h, and take 15 minutes as the time scale to take 16 sampling points for rolling optimization.

In order to verify the superiority of the multi-time-scale rolling optimal scheduling method, the multi-time-scale rolling optimal scheduling method for this problem is compared with the day-ahead scheduling results. The comparison of the daily output rolling optimization and adjustment effects of the power grid, the heat grid, and the gas grid is shown in Figures 8–10, respectively. In order to cope with the load fluctuation caused by the forecast error of the ultra-short-term time scale of renewable energy within the day, the day-ahead dispatch optimization method mainly purchases energy from the external main network, Intraday rolling optimization scheduling mainly uses energy storage equipment and the low response time characteristics of CCGPP to provide active support for the intraday demand

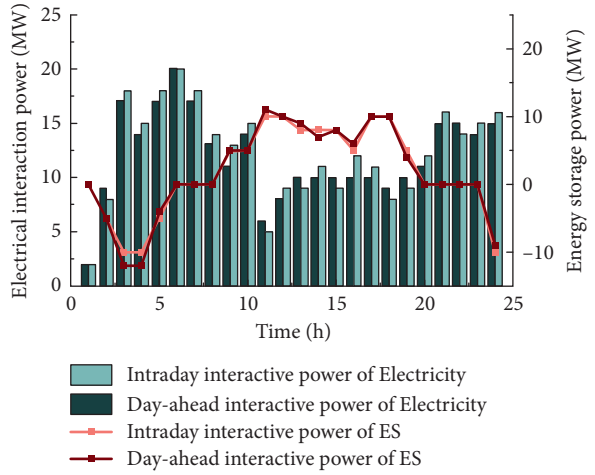

Figure 8: Intraday rolling dispatch adjustment effect of power grid.

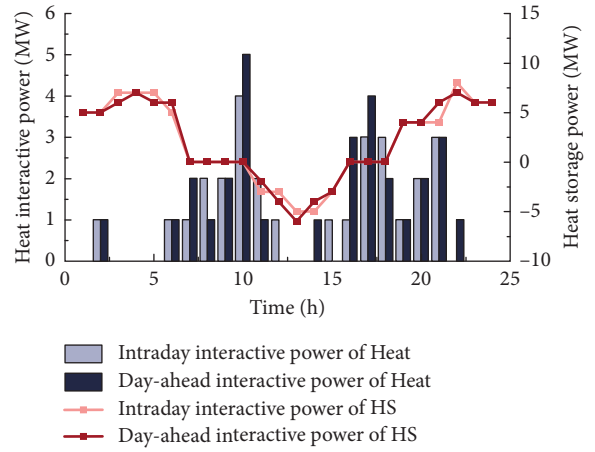

Figure 9: Intraday rolling scheduling adjustment effect of heat network.

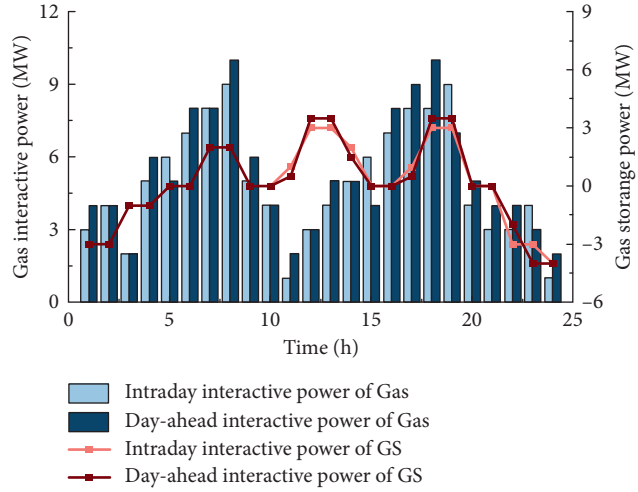

Figure 10: Intraday rolling scheduling adjustment effect of gas network.

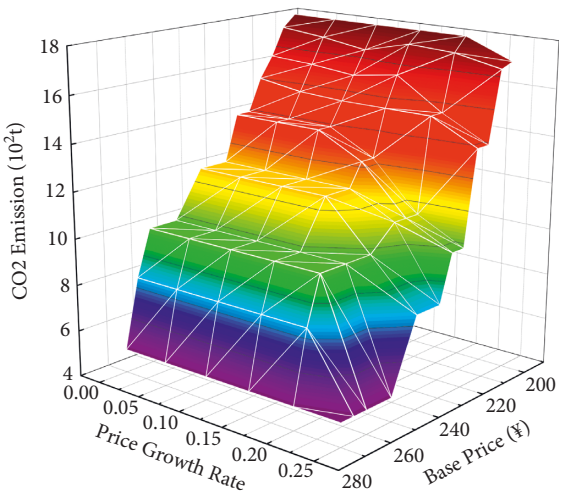

Figure 11: Carbon emission relationships for different base prices and price growth rates.

power of multiple loads. It ensures that the output adjustment is made on the basis of the effective scheduling plan before, and further eliminates the influence of the forecast error on the accuracy of the scheduling result.

According to the results of the daily rolling optimization, it can be seen that the energy purchased during the peak period of the load curve is reduced, and energy storage equipment is mainly used for adjustment. The rolling optimization scheduling results guide the energy storage device to perform more reasonable charging and discharging behaviors, so as to adjust the daily output in response to the source-load forecast error, and at the same time avoid the increase in loss costs caused by frequent charging and discharging, and ensure operational reliability.

The carbon emission relationship between different base prices and price growth rates is shown in Figure 11. It can be seen that with the increase in price growth rate, the correlation between carbon emissions and base price gradually increases. When the base price reaches 240, the relationship between carbon emissions and the price growth rate weakens, and when the base price reaches 270, the price growth rate has nothing to do with carbon emission allowances.

When the price growth rate is in the range of 0–0.25, with the increase in the price of carbon emission rights allowances, each production entity adjusts the output range of equipment to reduce carbon emissions. When the price growth rate is close to 0.25, the output of the equipment is stable and at the lower limit of the adjustable range, and there is no longer an adjustment margin. At this time, the difference between carbon emission and carbon emission right quota is at the boundary of carbon emission interval, and increasing the price growth rate cannot effectively restrain carbon emission. It can be seen from the above analysis that when the difference between carbon emission and carbon emission right quota exceeds the carbon emission range, the price growth rate can constrain carbon emission to a certain extent.

6. Conclusions

In this study, a multi-time-scale rolling optimization model with the lowest comprehensive operating cost of NZCP as the optimization goal is established based on the stepped carbon emission allowance trading mechanism. The optimization results under the three scenarios are compared and analyzed to provide a theoretical basis for the construction of NZCP.

(1) A day-ahead-intraday rolling optimization model is established, the unit output plan is optimized in the day-ahead stage, and the output adjustment is formulated with local rolling optimization in the intraday stage. The fast response characteristics of energy storage equipment are fully utilized to participate in the intraday adjustment plan, which effectively reduces the cost of energy purchase and the operation and maintenance cost of energy storage devices, thereby reducing the operating cost of the system.

(2) The stepped carbon allowance trading mechanism is proposed and the carbon allowance compensation coefficient is introduced, which verifies that its carbon emission restraint efficiency and economy are better than the unified carbon allowance trading mechanism. Combined with the low-carbon characteristics of the CCGPP-P2G system, it provides a good economy for the system while offsetting carbon emissions.

(3) The carbon emission relationship between different base prices and price growth rates is analyzed. The difference between carbon emissions and carbon emission rights quotas should be within the length of the carbon emission range, and rationally setting price growth rates and base prices is conducive to constraining system carbon emissions within the total carbon allowances.

Data Availability

The datasets generated for this study are available on request to the corresponding author.

Conflicts of Interest

The authors declare that the research was conducted in the absence of any commercial or financial relationships that could be construed as potential conflicts of interest.

Acknowledgments

This work was supported by Key R&D Program of Liaoning Province (2020JH2/10300101), Liaoning Revitalization Talents Program (XLYC1907138), and Key R&D Program of Shenyang (GG200252).

References

[1] H. Li, N. Zhang, C. Kang, G. H. Xie, and Q. H. Li, "Analytics of contribution degree for renewable energy accommodation

factors," *Proceedings of the CSEE*, vol. 39, no. 4, pp. 1009–1018, 2019.

[2] Y. Cheng, E. Du, X. Tian, N. Zhang, and C. Q. Kang, "Carbon capture power plants in power systems: review and latest research trends," *Journal of Global Energy Interconnection*, vol. 3, no. 4, pp. 339–350, 2020.

[3] Y. Li, H. Zhang, X. Liang, and, B. Huang, "Event-triggered-based distributed cooperative energy management for multienergy systems," *IEEE Transactions on Industrial Informatics*, vol. 15, no. 4, pp. 2008–2022, 2019.

[4] Y. Li, D. W. Gao, W. Gao, H. Zhang, and J. Zhou, "A distributed double-Newton descent algorithm for cooperative energy management of multiple energy bodies in energy internet," *IEEE Transactions on Industrial Informatics*, vol. 17, no. 9, pp. 5993–6003, 2021.

[5] National Development and Reform Commission, "National Energy Board. Notice on printing and distributing the "14th Five-Year Plan for Modern Energy System" [EB/OL]," 2022, https://www.ndrc.gov.cn/xwdt/tzgg/202203/t20220322_1320017.html?code=&state=123.

[6] R. Wang, Q. Sun, P. Tu, J. Xiao, Y. Gui, and P. Wang, "Reduced-order aggregate model for large-scale converters with inhomogeneous initial conditions in DC microgrids," *IEEE Transactions on Energy Conversion*, vol. 36, no. 3, pp. 2473–2484, 2021.

[7] X. Li, R. Zhang, L. Bai, G. Li, T. Jiang, and H. Chen, "Stochastic low-carbon scheduling with carbon capture power plants and coupon-based demand response," *Applied Energy*, vol. 210, pp. 1219–1228, 2018.

[8] R. Wang, Q. Sun, W. Hu, Y. Li, D. Ma, and P. Wang, "SoC-based droop coefficients stability region analysis of the battery for stand-alone supply systems with constant power loads," *IEEE Transactions on Power Electronics*, vol. 36, no. 7, pp. 7866–7879, 2021.

[9] T. Ma, Z. Zhang, and B. Cui, "Impulsive consensus of nonlinear fuzzy multi-agent systems under DoS attack," *Nonlinear Analysis: Hybrid Systems*, vol. 44, Article ID 101155, 2022.

[10] T. Qin, H. Liu, J. Wang, Z. Feng, and W. Fang, "Carbon trading based low-carbon economic dispatch for integrated electricity-heat-gas energy system," *Automation of Electric Power Systems*, vol. 42, no. 14, pp. 8–13, 2018.

[11] Z. Chen, Z. Hu, C. Weng, and T. Li, "Multi-stage planning of park-level integrated energy system based on ladder-type carbon trading mechanism," *Electric Power Automation Equipment*, vol. 41, no. 9, pp. 148–155, 2021.

[12] N. Li, W. Wang, X. Ma, F. Li, F. Yang, and X. Li, "Distribution network expansion planning considering carbon trading cost and regional energy optimization," *Science Technology and Engineering*, vol. 22, no. 8, pp. 3101–3109, 2022.

[13] Z. Wang, Y. Teng, H. Hu, and Z. Chen, "Multi-energy system optimal model in consideration of coordinate disposal of power grid and gas network and waste," *High Voltage Engineering*, vol. 47, no. 1, pp. 63–72, 2021.

[14] Y. Teng, P. Sun, M. Zhang, Z. Chen, Robust optimization model of "Energy-environment-economy" based on the new rural industrial structure," *Proceedings of the CSEE*, vol. 42, no. 2, pp. 614–631, 2022.

[15] H. Yang, M. Xie, W. Huang, M. Zhang, B. Shi, Y. Hong, Z. Zhu, and W. Yu, Low-carbon economic operation of urban integrated energy system including waste treatment," *Power System Technology*, vol. 45, no. 9, pp. 3545–3552, 2021.

[16] C. Wang, C. Lv, P. Li, L. Shuquan and Z. Kunpeng, Multiple time-scale optimal scheduling of community integrated energy system based on model predictive control," *Proceedings of the CSEE*, vol. 39, no. 23, pp. 6791–6803+7093, 2019.

[17] X. Jin, Y. Mu, H. Jia, X. D. Yu, K. Xu, and J. Xu, "Model predictive control based multiple-time-scheduling method for microgrid system with smart buildings integrated," *Automation of Electric Power Systems*, vol. 43, no. 16, pp. 25–33, 2019.

[18] J. Tang, M. Ding, S. Lu, S. Li, J. Huang, and W. Gu, "Operational flexibility constrained intraday rolling dispatch strategy for CHP microgrid," *IEEE Access*, vol. 7, pp. 96639–96649, 2019.

[19] Z. Wang, S. Yan, Application of carbon capture technology in gas power plant," *Modern Chemical Industry*, vol. 38, no. 9, pp. 195–197, 2018.

[20] Q. Chen, C. Kang, and Q. Xia, "Operation mechanism and peak-load shaving effects of carbon-capture power plant," *Proceedings of the CSEE*, vol. 30, no. 7, pp. 22–28, 2010.

[21] Q. Chen, Z. Ji, C. Kang, and H. Ming, "Analysis on relation between power generation and carbon emission of carbon capture power plant in different operation modes," *Automation of Electric Power Systems*, vol. 36, no. 18, pp. 109–115, 2012.

[22] Y. Cui, P. Zeng, Z. Wang, M. Wang, J. Zhang, and Y. Zhao, "Low-carbon economic dispatch of electricity-gas-heat integrated energy system that takes into account the electricity price-type demand-side response to carbon-containing capture equipment," *Power System Technology*, vol. 45, no. 2, pp. 447–461, 2021.

[23] R. Wang, Q. Sun, D. Ma, and Z. Liu, "The small-signal stability analysis of the droop-controlled converter in electromagnetic timescale," *IEEE Transactions on Sustainable Energy*, vol. 10, no. 3, pp. 1459–1469, 2019.

[24] S. Clegg, and P. Mancarella, "Integrated modeling and assessment of the operational impact of power-to-gas (P2G) on electrical and gas transmission networks," *IEEE Transactions on Sustainable Energy*, vol. 6, no. 4, pp. 1234–1244, 2015.

[25] A. T. Sipra, N. Gao, and H. Sarwar, "Municipal solid waste (MSW) pyrolysis for bio-fuel production: a review of effects of MSW components and catalysts," *Fuel Processing Technology*, vol. 175, pp. 131–147, 2018.

[26] N. A. Qambrani, M. M. Rahman, S. Won, S. Shim, and C. Ra, "Biochar properties and eco-friendly applications for climate change mitigation, waste management, and wastewater treatment: a review," *Renewable and Sustainable Energy Reviews*, vol. 79, pp. 255–273, 2017.

[27] N. Scarlat, J. F. Dallemand, and F. Fahl, "Biogas: developments and perspectives in europe," *Renewable Energy*, vol. 129, pp. 457–472, 2018.